iScience

CellPress
OPEN ACCESS

Article

Cytoplasmic proteotoxicity regulates HRI-dependent phosphorylation of eIF2α via the Hsp70-Bag3 module

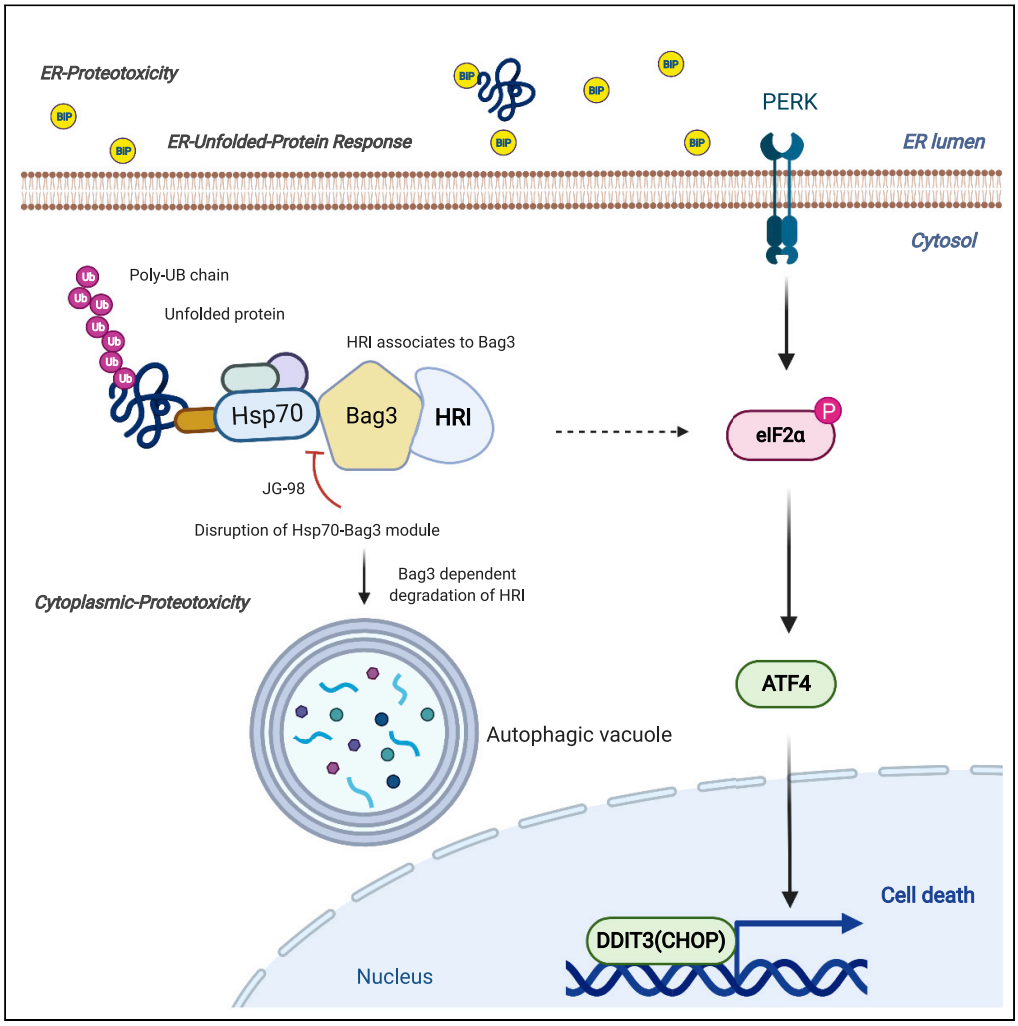

Shivani Patel, Santosh Kumar, Simone Baldan, Arkadi Hesin, Julia Yaglom, Michael Y. Sherman

sherma1@ariel.ac.il

Highlights

Disruption of Hsp70-Bag3 module activates the unfolded protein response (UPR)

This induction of UPR genes is mediated by HRI-dependent phosphorylation of eIF2α

Hsp70-Bag3 "monitors" cytoplasmic proteotoxicity to activate the HRI-eIF2α axis

eIF2α integrates proteotoxicity signals from ER and cytoplasm

Patel et al., iScience 25, 104282
May 20, 2022
https://doi.org/10.1016/j.isci.2022.104282

iScience

CellPress
OPEN ACCESS

Article

Cytoplasmic proteotoxicity regulates HRI-dependent phosphorylation of eIF2α via the Hsp70-Bag3 module

Shivani Patel,[1,2] Santosh Kumar,[1] Simone Baldan,[1] Arkadi Hesin,[1] Julia Yaglom,[1] and Michael Y. Sherman[1,*]

SUMMARY

The major heat shock protein Hsp70 forms a complex with a scaffold protein Bag3 that links it to components of signaling pathways. Via these interactions, the Hsp70-Bag3 module functions as a proteotoxicity sensor that controls cell signaling. Here, to search for pathways regulated by the complex, we utilized JG-98, an allosteric inhibitor of Hsp70 that blocks its interaction with Bag3. RNAseq followed by the pathway analysis indicated that several signaling pathways including UPR were activated by JG-98. Surprisingly, only the eIF2α-associated branch of the UPR was activated, while other UPR branches were not induced, suggesting that the response was unrelated to the ER proteotoxicity and ER-associated kinase PERK1. Indeed, induction of the UPR genes under these conditions was driven by a distinct eIF2α kinase HRI. Hsp70-Bag3 directly interacted with HRI and regulated eIF2α phosphorylation upon cytoplasmic proteotoxicity. Therefore, cytosolic proteotoxicity can activate certain UPR genes via Hsp70-Bag3-HRI-eIF2α axis.

INTRODUCTION

The major heat shock protein Hsp70 has been implicated in cancer development (Calderwood et al., 2006; Mosser and Morimoto, 2004; Sherman and Gabai, 2015). Original hypothesis was that cancer cells experience permanent proteotoxicity stress due to aneuploidy, oxidative stress, and other abnormalities, which dictates their stronger requirements for expression of molecular chaperones (non-oncogene addiction) compared to normal cells (Donnelly and Storchová, 2015; Solimini et al., 2007). This hypothesis was generally refuted (Teresa A Colvin et al., 2014), which led to the idea of direct involvement of Hsp70 in signaling pathways that control major stages of cancer development, including initiation, progression, and metastasis. Indeed, several publications demonstrated that knockout of Hsp70 leads to suppression of cancer development at various stages (depending on the cancer model) and these effects correlated with suppression of many signaling pathways involved in cancer development (Cho et al., 2019; Gong et al., 2015; Meng et al., 2011; Tao et al., 2016).

We and others previously reported that effects of Hsp70 on signaling pathways are mediated by the co-chaperone Bag3 that binds to the ATPase domain of Hsp70 and links it to components of various signaling pathways, like Src, Hif1, NF-kB, p53, Hippo, and others (Albakova et al., 2020; Ammirante et al., 2010; Teresa A. Colvin et al., 2014; Doong et al., 2000; Falco et al., 2012; Gabai et al., 2012; Guerriero et al., 2017; Kathage et al., 2017, p. 1; Meriin et al., 2018; Rosati et al., 2012). Knockout or depletion of Hsp70 or Bag3 affected activities of these pathways, which significantly influenced cancer cell physiology (Teresa A. Colvin et al., 2014). With some of these pathways, direct interaction with Bag3 was reported, e.g. Src, Yes, or Lats1 (Teresa A. Colvin et al., 2014; Hiebel et al., 2020; Kögel et al., 2020), while with other pathways, e.g. Hif1 or FoxM1, mechanisms of effects of Hsp70 and Bag3 remain unclear.

Very importantly, knockout of Hsp70 did not significantly affect normal organism development and physiology, while strongly suppressing proliferation and survival of cancer cells (Gabai et al., 2009a; Yaglom et al., 2007). These and other findings made Hsp70 an attractive target for the anticancer drug design, and a number of attempts have been made to develop Hsp70 inhibitors as drug prototypes (Adam et al., 2014; Braunstein et al., 2011; Chang et al., 2011; Coşkun et al., 2021; Koren et al., 2010; Leu et al., 2009; Lu et al., 2006; Massey et al., 2010; Phillips et al., 2011; Pirali et al., 2020; Rérole et al., 2011; Wang

[1]Laboratory of Cancer Biology, Department of Molecular Biology, Ariel University, Ariel, 40700, Israel

[2]Lead contact

*Correspondence: sherma1@ariel.ac.il

https://doi.org/10.1016/j.isci.2022.104282

et al., 2021). Our collaborative work with the group of Jason Gestwicki reported a series of inhibitors of Hsp70, e.g. YM-01 or JG-98, that interact with an allosteric site at the ATPase domain of Hsp70 and freeze it in the ADP-bound form, which, in turn, leads to dissociation of Bag3 (Teresa A. Colvin et al., 2014; Li et al., 2015). These inhibitors mimicked all effects of Hsp70 depletion on a series of signaling pathways both in cell culture and in tumor xenograft animal models (Teresa A. Colvin et al., 2014; Li et al., 2015). Interestingly, other Hsp70 inhibitors that do not cause dissociation of Bag3 did not show these effects on signaling pathways (Teresa A. Colvin et al., 2014). Importantly, YM-01, JG-98, and more advanced inhibitors from this series, e.g. JG-231, demonstrated potent anticancer effects (Gabai et al., 2016; Moradi-Marjaneh et al., 2019; Shao et al., 2018; Yaglom et al., 2018). These effects were related to both direct suppression of growth of tumor cells and their death, as well as suppression of migration of tumor-associated macrophages into the tumor (Gabai et al., 2016). Further investigation uncovered that effects of this class of Hsp70 inhibitors are entirely different from effects of Hsp90 inhibitors and are clearly related to dissociation of the Hsp70-Bag3 complex (Yaglom et al., 2018). JG-98 and related inhibitors have been successfully used as chemical probes to investigate effects of Hsp70-Bag3 interaction on cell signaling, autophagy, protein degradation, aggregation, and other processes (Li et al., 2015).

Originally, effects of Hsp70-Bag3 on signaling were mostly studied by depletion of these proteins or inhibitors of their interaction, and normal physiological function of Hsp70-Bag3 complex in cell signaling was not clarified. Recently, we demonstrated the physiological role of the Hsp70-Bag3 module in sensing of the buildup of abnormal proteins in cells, and transmitting this signal to the downstream pathways (Meriin et al., 2018). As part of sensing abnormal proteins, Hsp70-Bag3 complex monitors the folding state of filamine A, which is involved in cell mechanosensing (Ulbricht et al., 2013).

In response to a stress environment, cells adjust their metabolic status through regulation of translation, called the integrated stress response (ISR) (Pakos-Zebrucka et al., 2016; Wek, 2018). These stresses involve accumulation of unfolded proteins in the ER, amino acid or glucose deprivation, heat shock, heme deprivation, oxidative stress, viral infection, and hypoxia (García et al., 2007; Han et al., 2001; Harding et al., 1999, 2003; McEwen et al., 2005; Pakos-Zebrucka et al., 2016; Ron, 2002), as well as oncogene activation during tumorigenesis (Denoyelle et al., 2006). Upon ISR, stress signals trigger kinases that activate phosphorylation of the alpha subunit of eukaryotic translation initiation factor 2 (eIF2α) on serine 51(Kimball et al., 2001a; Pakos-Zebrucka et al., 2016; Walter and Ron, 2011). This phosphorylation is facilitated by a family of four eIF2α kinases that are activated by distinct stress stimuli (Donnelly et al., 2013), such as PERK upon accumulation of unfolded proteins in ER (Harding et al., 1999), GCN2 upon amino acid deprivation (Castilho et al., 2014; Dever et al., 1992), PKR upon viral infection, oxidative stress, and ribotoxic stress (García et al., 2006, 2007; Meurs et al., 1990), and HRI upon a broad range of proteotoxic stresses, including heme deprivation, oxidative and osmotic stress, heat shock, and proteasome inhibition (Chen et al., 1991; Chen and Zhang, 2019; McEwen et al., 2005; Yerlikaya et al., 2008).

Recent study demonstrated that HRI is involved in clearing cytosolic protein aggregates upon inhibition of ubiquitin-proteasome system (Mukherjee et al., 2021). Furthermore, silencing of HRI resulted in decreased levels of BAG3 and HSPB8, two proteins involved in chaperone-assisted selective autophagy. Therefore, HRI may play an important role in cytosolic proteostasis through chaperone-assisted selective autophagy. However, mechanisms of activation of HRI by the cytosolic proteotoxicity remain unclear. We hypothesized that Hsp70-Bag3 complex that regulates responses of stress kinases to proteotoxicity (Baldan et al., 2021; Meriin et al., 2018) may be involved in regulation of HRI.

Here, we analyzed effects of the disruption of Hsp70-Bag3 complex on the transcriptome to identify pathways regulated by this complex. This line of investigation led to understanding the role of the Hsp70-Bag3 complex in transmitting the cytoplasmic proteotoxicity signal to the HRI-eIF2α axis. Accordingly, eIF2α integrates the proteotoxicity signals both from ER via BiP and PERK1, and from cytoplasm via Hsp70-Bag3-HRI.

RESULTS

Inhibition of Hsp70 by JG-98 induces UPR genes

To obtain insights about signaling pathways regulated by the Hsp70-Bag3 module, we assessed how disruption of this complex up- or downregulates signaling using the RNAseq analysis, followed by the pathway analysis. MCF10A cells were incubated either with 1uM JG-98, a small molecule that inhibits

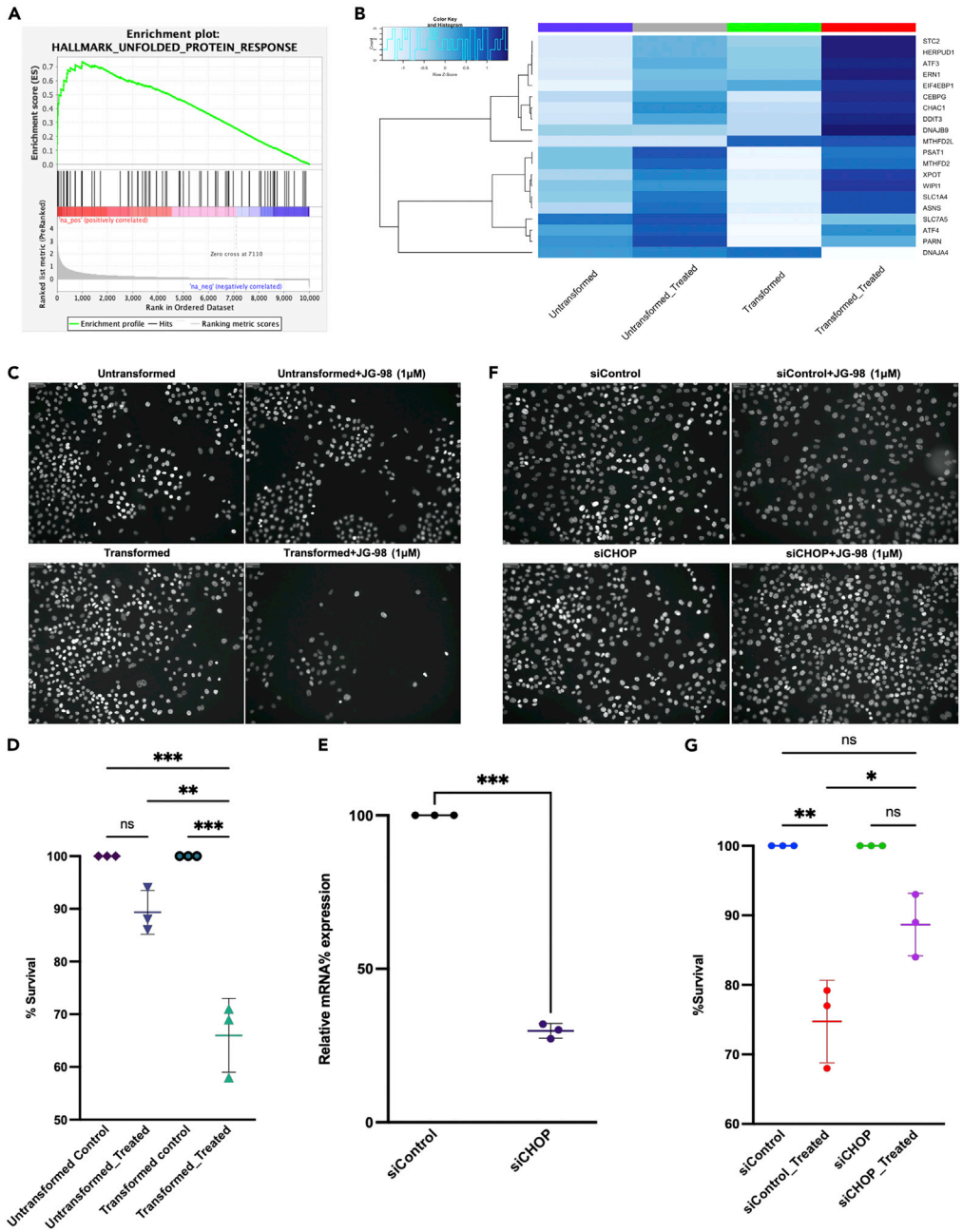

Figure 1. Her2 transformed cells showed upregulation of UPR genes in response to JG98

Transformation with Her2 oncogene enhances the sensitivity of the MCF10A cells to JG-98 treatment. Transcriptome analysis was performed with untransformed and transformed MCF10A cells treated with 1 μM JG-98 treatment for 12 h or left untreated.

(A) GSEA analysis of RNAseq data shows significant upregulation of UPR pathway following JG-98 treatment.

(B) Hallmark genes of unfolded protein response are significantly enriched in transformed cells in response to JG-98 treatment compared to untransformed cells. Color key represents the raw *Z* score. The experiments were performed in biological duplicates (n = 2).

(C) Sensitivity of transformed and untransformed cells to JG-98. MCF10A or Her2-transformed MCF10A cells were treated with 1 μM JG-98 for 24 h at 50% confluency or left untreated. Cell viability was counted by number of DAPI stained cells using Hermes Imaging systems (representative images shown). Experiment was performed in biological replicates (n = 3) and high throughput analysis was done using 31 images from each well using in-built Athena software package.

Figure 1. *Continued*
(D) Scatterplot showing the relative percentage of cells survival after 24 h of JG-98 treatment with means ± SEM (Quantification of data shown in (C)). Statistical analysis was performed using two-way ANOVA.
(E) Efficiency of CHOP (DDIT3) depletion following siRNA treatment. Levels of CHOP mRNA were quantified by qPCR, experiment was performed in biological replicates (n = 3), scatterplot showing the relative mRNA depletion represented as means ± SEM, statistics was performed using unpaired Welch's correction, two-tailed t-test.
(F) CHOP depletion reduces cell death in response to JG-98. Cells were transfected with siControl or siCHOP, followed by 1μM of JG-98 treatment for 24 h or left untreated. Cell viability was counted by number of DAPI stained cells using Hermes Imaging systems and representative images shown, experiment was performed in biological replicates (n = 3) and analysis was done using 126 images from each well.
(G) Scatterplot showing relative percentage of cells survival after 24 h of JG-98 treatment plotted as means ± SEM (Quantification of data shown in (F)), Statistical analysis was performed using two-way ANOVA. All statistical analysis was performed using Graphpad (v9), level of significance was taken as (*p < 0.0332, **p < 0.0021, ***p < 0.0002). See also Figures S1·S2, and Tables S1–S3.

Hsp70 and disrupts Hsp70-Bag3 complex, for 12 h or remained untreated and RNA was isolated and sent for sequencing. After normalization of the results, we performed GSEA pathway analysis (See also Table S1). As expected, we found that pathways related to the cell cycle changes, e.g. E2F targets, G2/M and myc targets, were significantly downregulated. Among significantly upregulated pathways, we found UPR (Figure 1A), which was represented by a set of genes, including ATF3, ATF4, CHAC1, CHOP (DDIT3), and others (Figure 1B).

In these experiments, we compared gene expression profiles in response to JG-98 of normal MCF10A cells and MCF10A transformed with a single oncogene Her2. To transform, cells were infected with a retrovirus expressing neu mutant form of Her2 oncogene (See also Figure S1), which significantly changed their phenotype from epithelial to more mesenchymal (not shown). In parallel, RNAseq analysis indicated that the entire set of cancer-related pathways was upregulated by Her2 (See also Figure S2).

Interestingly, expression of most of the UPR genes, was upregulated more strongly by JG-98 in Her2-transformed cells compared to untransformed MCF10A (Figure 1B). Such enhanced induction of the UPR genes upon transformation correlated with the enhanced sensitivity to JG-98 (Figures 1C and 1D). This correlation suggested a link between induction of UPR and cell death, which was in line with the pro-apoptotic function of the CHOP (Tabas and Ron, 2011). Indeed, depletion of CHOP using the corresponding siRNA significantly protected cells from JG-98 (Figures 1E–1G).

Upregulation of this set of UPR genes suggested that in response to JG-98, the upstream regulator of the pathway a translation initiation factor eIF2α could become phosphorylated and thus inactivated, which we indeed observed (Figures 2A and 2B). In line with stronger induction of the UPR genes, phosphorylation of eIF2α was also activated more strongly by JG-98 in Her2-transformed cells (Figure 2A), further supporting the idea that the entire pathway is activated.

Phosphorylation of eIF2α and induction of UPR genes associate with inhibition of Hsp70-Bag3

Activation of UPR suggested that JG-98 could cause a buildup of abnormal proteins in the endoplasmic reticulum. However, analysis of the RNAseq data suggested that this possibility is not the case. eIF2α phosphorylation represents only one out of three branches of the UPR response, which is regulated by the ER-associated PERK1 kinase (Harding et al., 2000). All three branches of UPR respond to titration of BiP by damaged polypeptides (Bergmann and Molinari, 2018). Two other branches that are controlled by other ER-associated signaling proteins IRE1 and ATF6 (Adams et al., 2019), regulate expression of distinct sets of genes, e.g. ER chaperones. Surprisingly, among genes upregulated by JG-98, there were no ER chaperones or other genes regulated by either IRE1 or ATF6 (See also Table S2). Accordingly, it was unlikely that effects of JG-98 could be associated with inhibition of BiP and accumulation of abnormal proteins in ER.

Overall, using JG-98 as a chemical probe for assessing effects of disruption of the Hsp70-Bag3 complex has a general drawback since this reagent can inhibit not only cytoplasmic Hsp70 but also a variety of Hsp70 family members, including mitochondrial Hsp70 or ER-resident BiP (Li et al., 2015; Yaglom et al., 2018), which mediates the UPR in response to the buildup of abnormal proteins in the ER (Adams et al., 2019;

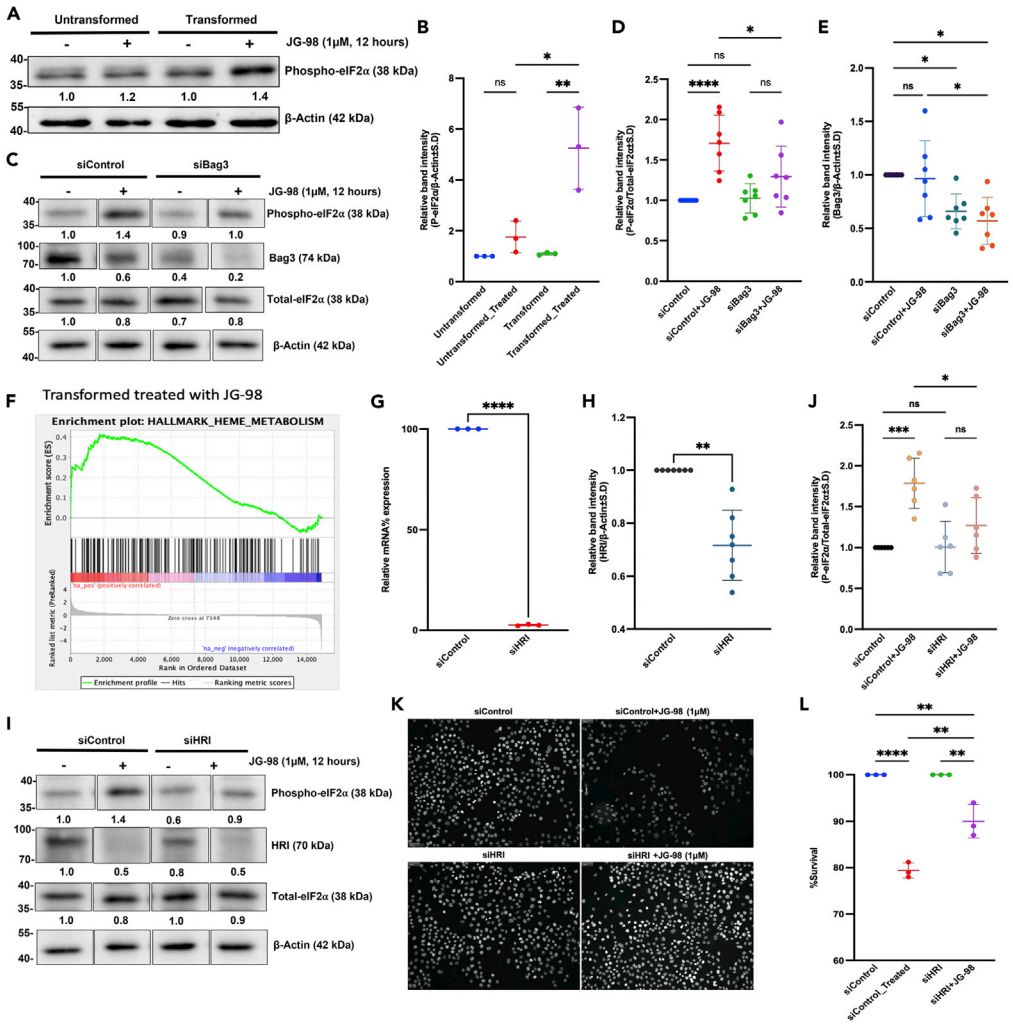

Figure 2. Phosphorylation of translation initiation factor eIF2α in response to JG-98 is mediated by Hsp70-Bag3-HRI complex

(A) Treatment by JG-98 strongly stimulates phosphorylation of eIF2α in Her2-transformed cells compared to untransformed cells. Cells were treated with 1 μM JG-98 for 12 h or left untreated. Levels of phospho-eIF2α were determined in cell lysates by immunoblotting with the corresponding antibody, independent experiments were performed three times (n = 3).

(B) Quantification of experiment presented in (A). Quantification of the relative band intensity was performed using ImageJ where β-actin served as loading controls. Scatterplot showing individual data points for n = 3 as means ± SEM, Statistical analysis was performed using two-way ANOVA.

(C) Depletion of Bag3 significantly reduced phosphorylation of eIF2α in the presence of JG-98. Untransformed cells were transfected with siBag3 or siControl and further treated by JG-98 (1uM, 12 h) or left untreated. Levels of phospho-eIF2α, Bag3, and total-eIF2α were determined in cell lysates by immunoblotting with corresponding antibody, independent experiments were performed seven times (n = 7), Raw data for corresponding cropped images are provided separately as a supplement (PAGE #3&4, file: Data S1).

(D) and (E) Quantification of experiment presented in Figure 2C. Quantification of the relative band intensity for (D) p-eIF2α and (E) Bag3 was performed using ImageJ where β-actin served as loading controls. Scatter plot showing individual data points for n = 7 as means ± SEM, Statistical analysis was performed using two-way ANOVA.

(F) GSEA analysis showing upregulation of the Heme metabolism pathway in response to JG-98 treatment.

(G) Efficiency of HRI depletion following siRNA treatment. Levels of HRI mRNA were quantified by qPCR, experiments were performed in biological replicates (n = 3) shown as means ± SEM, statistics was performed using unpaired Welch's correction, two-tailed t-test.(H) Protein levels for HRI was also checked using immunoblotting, statistics was performed unpaired Welch's correction, two-tailed t-test (n = 7) plotted as means ± SEM, representative images are available in supplement section.

Figure 2. *Continued*

(I) Depletion of HRI led to significant suppression of eIF2α phosphorylation in presence of JG-98. Untransformed cells were transfected with siHRI or siControl and further treated by JG-98 (1uM, 12 h) or left untreated. Levels of phospho-eIF2α, HRI, and total-eIF2α were determined in cell lysates by immunoblotting with the corresponding antibody, experiment was performed six times (n = 6). siControl of siBag3 and siHRI is same as experiment was conducted together and were immunoblotted on the same membrane, Raw data for corresponding cropped images are provided separately as a supplement (Page #5&6, file: Data S1).

(J) Quantification of the relative band intensity for p-eIF2α was performed. Scatter plot showing individual data points for n = 6 as means ± SEM, Statistical analysis was performed using two-way ANOVA.

(K) HRI depletion reduces cell death in response to JG-98. Untransformed cells were transfected with siControl and siHRI to silence HRI followed by 1 μM JG-98 treatment for 24 h or left untreated. Cell survival was evaluated by Hermes Imaging of DAPI-stained cells.

(L) Statistical analysis was performed by two-way ANOVA, n = 3 shown as means ± SEM Quantification of the blot was performed using ImageJ and OD ratios for each protein compared to the reference after normalization is added below each blot. Specifically, phospho-eIF2α was normalized additionally by total-eIF2α. All statistical analysis was performed using Graphpad (v9), level of significance was taken as (*p < 0.0332, **p < 0.0021, ***p < 0.0002, ****p < 0.0001). See also Figures S3–S7.

Haeri and Knox, 2012). Therefore, to test for the role the Hsp70-Bag3 complex, we used a genetic approach, i.e. siRNA depletion of Bag3. Indeed, Bag3 depletion significantly reduced JG-98-dependent upregulation of eIF2α phosphorylation (Figures 2C–2E). Importantly, expression of the siRNA-resistant version of Bag3 completely reversed the effect of the Bag3 siRNA on JG-98-dependent phosphorylation of eIF2α (See also Figure S3), further supporting the role of Bag3 in this process. These data strongly suggest that the main effect of JG-98 on phosphorylation of eIF2α is due to the targeting of the cytoplasmic Hsp70-Bag3 complex.

Accordingly, phosphorylation of eIF2α under these conditions could be triggered not by the ER-associated kinase PERK1 (which is co-regulated with IRE1 and ATF6) but by a distinct cytoplasmic kinase. Indeed, siRNA-mediated depletion of PERK1 did not affect JG-98-induced phosphorylation of eIF2α (See also Figures S4A and S4B). There are three known kinases in addition to PERK1 that can phosphorylate eIF2α, including a heme-responsive kinase HRI, an amino acid starvation-regulated kinase GCN2, and a double-strand RNA kinase PKR (Kimball et al., 2001b; Lu et al., 1999). An important insight to distinguish between effects of these kinases came from the GSEA analysis that showed a significant upregulation of the heme metabolism pathway in response to JG-98 (Figure 2F), suggesting that HRI is activated.

To test for the role of HRI in phosphorylation of eIF2α following JG-98 treatment, we knocked down HRI using corresponding siRNA (Figures 2G and 2H) and tested for the ability of JG-98 to facilitate phosphorylation of eIF2α. Indeed, depletion of HRI led to a significant downregulation of eIF2α phosphorylation in response to JG-98 (Figures 2I and 2J). Similar result was obtained with a distinct siRNA against HRI (See also Figure S5). Importantly, depletion of other eIF2α kinases GCN2 or PKR did not affect phosphorylation of eIF2α following treatment with JG-98 (See also Figures S6 and S7). Therefore, HRI appears to be the major kinase that controls phosphorylation of eIF2α upon disruption of Hsp70-Bag3 complex by JG-98. In line with the role of CHOP in JG-98-triggered cell death, depletion of HRI also demonstrated significant protection of cells from JG-98 (Figures 2K and 2L).

Cytoplasmic Hsp70-Bag3 associates with HRI and transmits proteotoxicity signals to HRI-eIF2α axis

Because the major role of the Hsp70-Bag3 module is transmitting signals about the buildup of abnormal proteins in the cytoplasm to a variety of pathways, we suggested that this module transmits the proteotoxicity signals to the HRI- eIF2α axis. Accordingly, we tested if triggering proteotoxicity by the proteasome inhibition can activate this axis in a Bag3-dependent manner. MCF10A cells were exposed to the proteasome inhibitor MG132 and eIF2α phosphorylation assessed either in control cells or cells depleted of HRI or Bag3. Similar to JG-98, depletion of either HRI or Bag3 significantly suppressed phosphorylation of eIF2α in response to proteasome inhibition (Figures 3A–3D). Therefore, the proteotoxic stress in the cytoplasm can signal to phosphorylate eIF2α via Hsp70-Bag3-HRI axis. This conclusion was in line with previous report that HRI can associate with Hsp70 (Thulasiraman et al., 1998, 2002) (possibly via Bag3, see below).

The role of Hsp70-Bag3 in regulation of HRI suggested that the latter can physically associate with Bag3. To test this possibility, we expressed in cells 6His-tagged Bag3, and pulled it down together with the

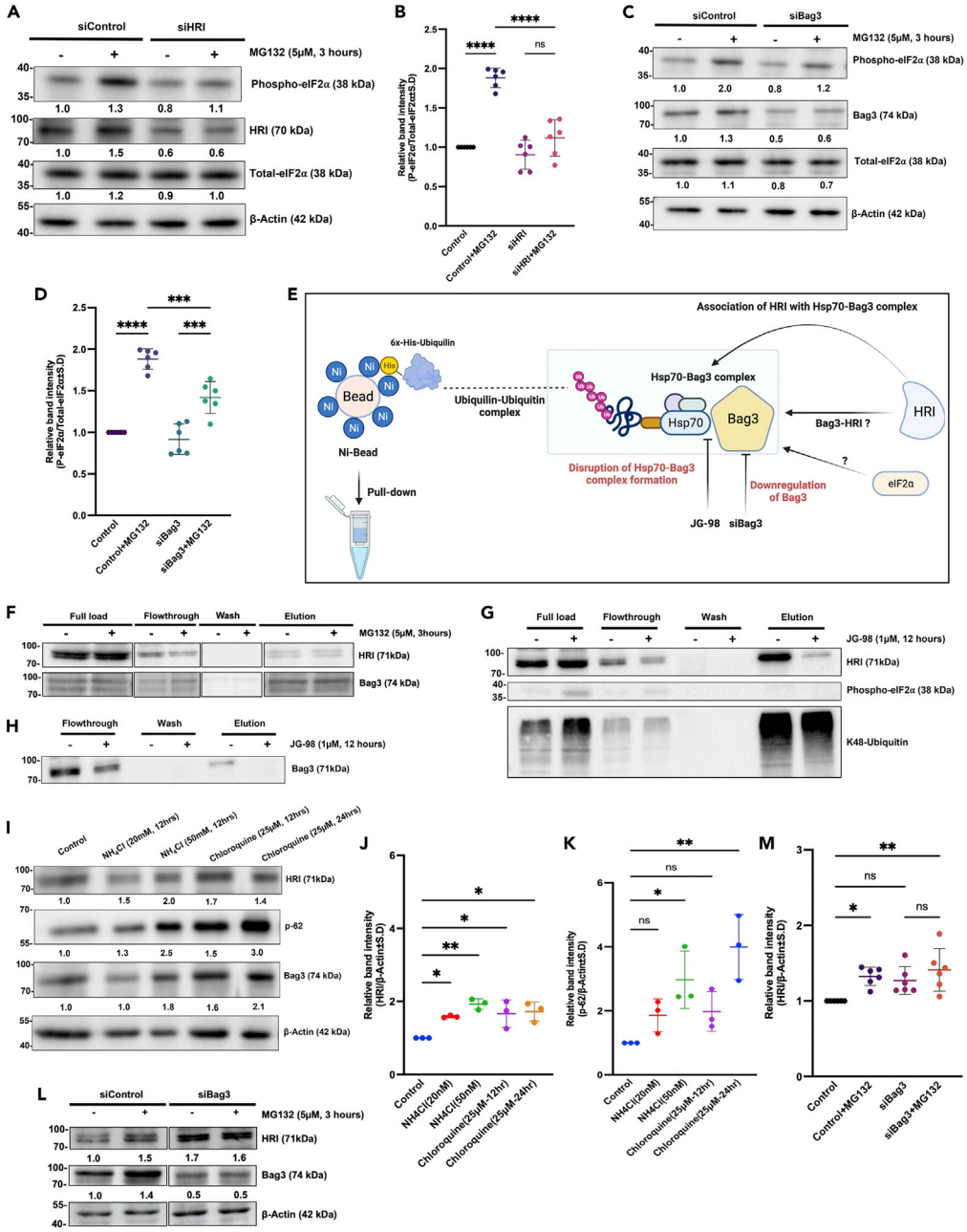

Figure 3. Proteotoxic stress in the cytoplasm signal to phosphorylate eIF2α via Hsp70-Bag3- HRI axis

(A) Depletion of HRI reduces phosphorylation of eIF2α in response to MG132. Cells were transfected with siHRI or siControl and further were treated by MG132 (5uM, 3 h) or left untreated. Levels of phospho-eIF2α were determined in cell lysates by immunoblotting with the corresponding antibody, experiment was performed independently for six times (n = 6).

(B) Scatterplot representation of individual data points for the change in phosphorylation of eIF2α in response to MG132 upon HRI depletion (shown as means ± SEM).

(C) Depletion of Bag3 significantly reduced phosphorylation of eIF2α in the presence of MG132. Experimental conditions were as in (A) and were performed six times independently (n = 6).

(D) Scatterplot representation of individual data points for the change in phosphorylation of eIF2α in response to MG132 upon Bag3 depletion, shown as means ± SEM.

(E) Schematic layout for the pulldown experiment to check the association of HRI, eIF2α to Hsp70-Bag3 complex. Parallel validation was performed by silencing the Bag3 or disrupting the Hsp70-Bag3 complex via JG-98.

Figure 3. *Continued*

(F) HRI associates with Bag3 in the pulldown assay. Association of HRI with Bag3 was assessed by expressing 6x-His-tagged Bag3-Full length and pulled it down together with associated proteins from naive cells and cells treated with MG132 for 3 h. The pulled down fraction was immunoblotted with anti-HRI antibody.

(G) Disruption of Hsp70-Bag3 complex leads to dissociation of HRI from ubiquitinated proteins. Cells were treated with JG-98 to disrupt Hsp70-Bag3 complex or left untreated. Ubiquitinated proteins were pulled down from these cells' extracts using ubiquilin-1 affinity column (see STAR Methods) and HRI, phospho-eIF2α levels in the pulldowns were measured by immunoblotting.

(H) Level of Bag3 was checked in pulldown samples by immunoblotting. Bag3 was not pulled down in elution upon JG98 treatment.

(I) Inhibition of autophagy by hydroxycholoquine or NH_4Cl increases HRI levels. Cells were treated with indicated concentrations of the inhibitors for indicated time periods, and levels of HRI, p62, and Bag3 were assessed by immunoblotting. Experiments were performed in biological replicates (n = 3).

(J and K) Scatterplot representation of individual data points for the change in HRI and p62 levels shown as means ± SEM.

(L and M) HRI levels are increased upon Bag3 depletion, experiments were performed independently six times (n = 6), Scatterplot representation of individual data points for the change in HRI shown as means ± SEM. All quantifications of the blots were performed using ImageJ and OD ratios for each protein compared to the reference after normalization was calculated. In case of phosphor-eIF2α, additional normalization was performed against total eIF2α. All statistical analysis was performed using Graphpad (v9), In this figure, section two-way ANOVA was used to compute level of significance and taken as (*$p < 0.0332$, **$p < 0.0021$, ***$p < 0.0002$, ****$p < 0.0001$). See also Figure S8.

associated proteins either from naive cells or cells treated with MG132 (Figure 3E). HRI was clearly pulled down in this experiment (Figure 3F), and addition of MG132 did not significantly affect its association with Bag3 (Figure 3F), indicating that regulation of eIF2α phosphorylation by proteotoxic stress does not involve dissociation of HRI from Bag3.

Overall, these data suggested that regulation of HRI activity by the buildup of abnormal proteins in the cytosol is mediated by interaction with the Hsp70-Bag3 module. Accordingly, Hsp70-Bag3 could serve as a physical link between HRI and abnormal ubiquitinated proteins. In other words, ubiquitinated proteins associate with Hsp70, which interacts with Bag3, which recruits HRI into the complex. This model predicts that disruption of the Hsp70-Bag3 complex should break association of HRI with ubiquitinated proteins. Accordingly, we pulled down ubiquitinated proteins from the cells using affinity purification with the UBA domain of ubiquilin-1 and immunoblotted with anti-HRI antibody. Indeed, in naive cells, significant fraction of HRI associated with polyubiquitinated proteins (Figure 3G). However, disruption of Hsp70-Bag3 complex by JG-98 strongly reduced association of HRI with polyubiquitinated proteins (Figures 3G and 3H). Similar results were seen upon depletion of Bag3 (See also Figures S8A and S8B). Thus, Hsp70-Bag3 module mediates this interaction. Interestingly, we could not see eIF2α in these pulldowns (Figure 3G), suggesting that association of HRI and Bag3 with eIF2α is either weak or transient.

Association of HRI with Bag3 was in line with an unexpected finding that HRI can be degraded by autophagy. Indeed, incubation with the autophagic inhibitors hydroxychloroquine or NH_4Cl significantly increased the level of HRI (Figures 3I–3K). Previously, it was shown that Bag3 recruits certain types of cargo to the autophagic machinery (Carra et al., 2008; Ganassi et al., 2016), and considering that Bag3 depletion led to increase in the HRI levels, the autophagic degradation appeared to be mediated by Bag3 (Figures 3L and 3M). Therefore, Bag3 appears to interact with HRI and regulate HRI-dependent phosphorylation of eIF2α, as well as HRI degradation via the autophagic pathway.

Overall, these data uncovered a novel proteotoxicity signaling mechanism that involves Hsp70-Bag3-dependent activation of HRI, which mediates phosphorylation of eIF2α and triggers downstream events.

DISCUSSION

Here, we addressed which signaling pathways are regulated by Hsp70-Bag3 complex by investigating gene expression changes in response to an inhibitor of Hsp70-Bag3 interaction JG-98. Indeed, RNAseq followed by the pathway analyses predicted activation of UPR-related genes triggered by phosphorylation and inhibition of the translation initiation factor eIF2α. Because one of the genes in this pathway is a pro-apoptotic transcription factor CHOP, we suggested that its activation could contribute to the JG-98-induced cell death. Indeed, depletion of CHOP significantly protected cells from JG-98 treatment.

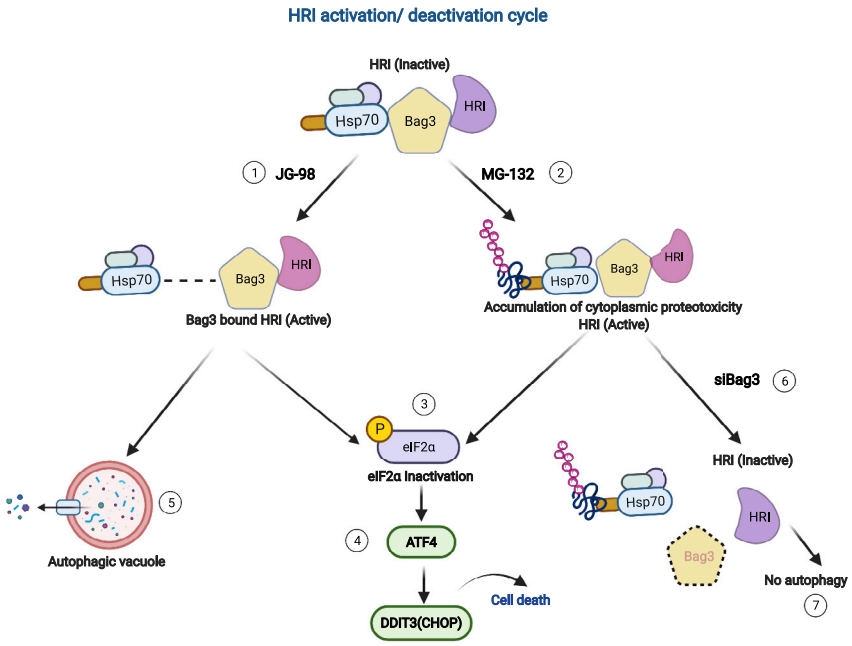

Figure 4. Model for Hsp70-Bag3-HRI

In resting state, Hsp70 holds the HRI with help of Bag3 and keeps it in inactive form. Further, after sensing proteotoxicity due to (1) disruption of complex Hsp70-Bag3 in presence of JG-98 or (2) in presence of MG-132 after inhibition of proteasome, HRI becomes active and (3) Bag3-HRI complex plays as key role to phosphorylate eIF2a. Further, this cascade of events leads to (4) selective translation of ATF4, followed by transcription of DDIT3(CHOP) leading to apoptosis. Separately, this complex (Bag3-HRI) is degraded through (5) autophagy. In another scenario, in case of (6) Bag3 depletion, accumulation of inactive form of HRI takes place in the system due to inhibition of (7) Bag3-mediated autophagic degradation.

We were puzzled by the lack of activation of other branches of UPR by JG-98, strongly suggesting the lack of ER proteotoxicity under these conditions. Accordingly, we suggested that there might be a distinct pathway activated by JG-98 that leads to phosphorylation of eIF2α. Indeed, a cytosolic kinase HRI significantly contributed to eIF2α phosphorylation under these conditions. HRI was associated with Bag3, and its level was regulated by Bag3-dependent autophagy.

Prior works reported that HRI is responsible for phosphorylation of eIF2α in response to proteasome inhibitors (Adams et al., 2019). Here, we confirm this observation, and demonstrate that this response to proteotoxicity in cytosol is mediated by Bag3, since Bag3 depletion significantly reduced the levels of eIF2α phosphorylation. In this pathway, Hsp70-Bag3 linked HRI with abnormal ubiquitinated polypeptides, since disruption of the Hsp70-Bag3 complex by JG-98 led to dissociation of HRI from the ubiquitinated species. Interestingly, this complex also seems to target HRI for autophagic degradation, since inhibition of autophagy or depletion of Bag3 increased HRI levels. Notably, in autophagy, Bag3 cooperates with a small heat shock protein HspB8 (Carra et al., 2008; Ganassi et al., 2016; Mukherjee et al., 2021). Because small heat shock proteins associate with Hsp70-Bag3 complex (Carra et al., 2008; Ganassi et al., 2016), joining with HspB8 may stimulate degradation of HRI.

Inhibition of Hsp70 by JG-98 activated HRI, while depletion of Bag3 prevented this effect, as well as activation of HRI by the proteotoxic stress. Accordingly, our model is that Bag3 interacts with HRI and links it to Hsp70. Hsp70 alone keeps HRI in a suppressed state, while binding to Hsp70 of abnormal proteins relieves this suppression and leads to activation of HRI. Maybe, it enhances interaction of HRI with its substrate eIF2a, similar to the mechanism of activation of Hippo pathway, where proteotoxic stress via Hsp70-Bag3 regulates interaction of a kinase Lats1 with its substrate Yap (Baldan et al., 2021). Addition of JG-98 dissociates Hsp70 from Bag3-HRI complex and thus relieves HRI suppression by Hsp70, resulting in a stronger phosphorylation of eIF2a (Figures 2A and 2C). Freeing up of the Bag3-HRI complex may also lead to enhancement of Bag3-dependent targeting of HRI to autophagy and the corresponding drop in

its level (Figure 2I). Accordingly, to observe enhanced phosphorylation of eIF2a despite the drop of the HRI levels, the overall activity of HRI should be enhanced very strongly. On the other hand, depletion of Bag3 using siBag3 reduces the interaction between HRI with Hsp70 alone or Hsp70-abnormal proteins complex, and thus inhibits activation of HRI by either JG-98 or MG132 (Figures 2C and 3C). In addition, depletion of Bag3 prevents autophagic targeting of HRI, and its levels increase (Figure 3L). Accordingly, upon depletion of Bag3, the activity of HRI is reduced despite its higher levels (Figure 4).

Interactions between Bag3 and HRI are even more complicated, since recent work demonstrated that HRI regulates Bag3 and HspB8-dependent autophagic degradation of aggregated proteins (Mukherjee et al., 2021). Therefore, HRI appears to be an integral part of response to the buildup of abnormal proteins that cooperates with Bag3 in signaling and autophagy upon proteotoxic stress.

Overall, this work uncovered a novel Hsp70-Bag3-HRI pathway that detects the buildup of abnormal proteins in the cytosol and regulates phosphorylation of eIF2α. In turn, eIF2α integrates proteotoxicity signals both from ER and cytosol (Summary figure).

Limitations of the study

As a paradigm of proteotoxicity, we used inhibition of proteasome, which leads to accumulation of abnormal newly synthesized polypeptides. It is unclear if other types of abnormal cytoplasmic proteins (e.g. heat-denatured proteins) signal via the same pathway.

STAR★METHODS

Detailed methods are provided in the online version of this paper and include the following:

- KEY RESOURCES TABLE
- RESOURCE AVAILABILITY
  - Lead contact
  - Materials availability
  - Data and code availability
- EXPERIMENTAL MODEL AND SUBJECT DETAILS
  - Cell culture
- METHOD DETAILS
  - Reagents and antibodies
  - Constructs and oligonucleotides
  - Real time PCR analysis
  - Virus preparation and infection
  - Immunofluorescence
  - Immunoprecipitation and immunoblotting
  - Raw images of immunoprecipitation and immunoblotting
  - Pull-down experiments
  - Data analysis
  - RNAseq processing
  - Data processing

SUPPLEMENTAL INFORMATION

Supplemental information can be found online at https://doi.org/10.1016/j.isci.2022.104282.

ACKNOWLEDGMENTS

Authors acknowledge that present work was supported by NIH Grant-R01 800000163 and Israel Science Foundation Grant: ISF-1444/18, ISF-2465/18.

AUTHOR CONTRIBUTIONS

Conceived, designed, and performed the experiments: S. Patel, S. Kumar, Data analysis: S. Patel, S. Kumar, additionally co-authors: S. Baldan and J. Yaglom have helped in additional experiments and are presented in the supplement section. A. Hesin has been involved in project administration, Manuscript preparation by: S. Patel, S. Kumar, M. Sherman.

DECLARATION OF INTERESTS

The authors declare that they have no conflicts of interest with the contents of this article.

Received: November 23, 2021
Revised: February 27, 2022
Accepted: April 19, 2022
Published: May 20, 2022

REFERENCES

Adam, C., Baeurle, A., Brodsky, J.L., Wipf, P., Schrama, D., Becker, J.C., and Houben, R. (2014). The HSP70 modulator MAL3-101 inhibits Merkel cell carcinoma. PLoS One *9*, e92041. https://doi.org/10.1371/journal.pone.0092041.

Adams, C.J., Kopp, M.C., Larburu, N., Nowak, P.R., and Ali, M.M.U. (2019). Structure and molecular mechanism of ER stress signaling by the unfolded protein response signal activator IRE1. Front. Mol. Biosci. *6*, 11. https://doi.org/10.3389/fmolb.2019.00011.

Albakova, Z., Armeev, G.A., Kanevskiy, L.M., Kovalenko, E.I., and Sapozhnikov, A.M. (2020). HSP70 multi-functionality in cancer. Cells *9*, 587. https://doi.org/10.3390/cells9030587.

Ammirante, M., Rosati, A., Arra, C., Basile, A., Falco, A., Festa, M., Pascale, M., d'Avenia, M., Marzullo, L., Belisario, M.A., et al. (2010). IKKγ protein is a target of BAG3 regulatory activity in human tumor growth. Proc. Natl. Acad. Sci. U S A. *107*, 7497–7502. https://doi.org/10.1073/pnas.0907696107.

Baldan, S., Meriin, A.B., Yaglom, J., Alexandrov, I., Varelas, X., Xiao, Z.-X.J., and Sherman, M.Y. (2021). The Hsp70-Bag3 complex modulates the phosphorylation and nuclear translocation of Hippo pathway protein Yap. J. Cell Sci. *134*, jcs259107. https://doi.org/10.1242/jcs.259107.

Bergmann, T.J., and Molinari, M. (2018). Three branches to rule them all? UPR signalling in response to chemically versus misfolded proteins-induced ER stress. Biol. Cell *110*, 197–204. https://doi.org/10.1111/boc.201800029.

Braunstein, M.J., Scott, S.S., Scott, C.M., Behrman, S., Walter, P., Wipf, P., Coplan, J.D., Chrico, W., Joseph, D., Brodsky, J.L., and Batuman, O. (2011). Antimyeloma effects of the heat shock protein 70 molecular chaperone inhibitor MAL3-101. J. Oncol. *2011*, 1–11. https://doi.org/10.1155/2011/232037.

Calderwood, S.K., Khaleque, M.A., Sawyer, D.B., and Ciocca, D.R. (2006). Heat shock proteins in cancer: chaperones of tumorigenesis. Trends Biochem. Sci. *31*, 164–172. https://doi.org/10.1016/j.tibs.2006.01.006.

Carra, S., Seguin, S.J., and Landry, J. (2008). HspB8 and Bag3: a new chaperone complex targeting misfolded proteins to macroautophagy. Autophagy *4*, 237–239. https://doi.org/10.4161/auto.5407.

Castilho, B.A., Shanmugam, R., Silva, R.C., Ramesh, R., Himme, B.M., and Sattlegger, E. (2014). Keeping the eIF2 alpha kinase Gcn2 in check. Biochim. Biophys. Acta *1843*, 1948–1968. https://doi.org/10.1016/j.bbamcr.2014.04.006.

Chang, L., Miyata, Y., Ung, P.M.U., Bertelsen, E.B., McQuade, T.J., Carlson, H.A., Zuiderweg, E.R.P., and Gestwicki, J.E. (2011). Chemical screens against a reconstituted multiprotein complex: myricetin blocks DnaJ regulation of DnaK through an allosteric mechanism. Chem. Biol. *18*, 210–221. https://doi.org/10.1016/j.chembiol.2010.12.010.

Chen, J.J., Throop, M.S., Gehrke, L., Kuo, I., Pal, J.K., Brodsky, M., and London, I.M. (1991). Cloning of the cDNA of the heme-regulated eukaryotic initiation factor 2 alpha (eIF-2 alpha) kinase of rabbit reticulocytes: homology to yeast GCN2 protein kinase and human double-stranded-RNA-dependent eIF-2 alpha kinase. Proc. Natl. Acad. Sci. U S A. *88*, 7729–7733. https://doi.org/10.1073/pnas.88.17.7729.

Chen, J.-J., and Zhang, S. (2019). Heme-regulated eIF2α kinase in erythropoiesis and hemoglobinopathies. Blood *134*, 1697–1707. https://doi.org/10.1182/blood.2019001915.

Cho, W., Jin, X., Pang, J., Wang, Y., Mivechi, N.F., and Moskophidis, D. (2019). The molecular chaperone heat shock protein 70 controls liver cancer initiation and progression by regulating adaptive DNA damage and mitogen-activated protein kinase/extracellular signal-regulated kinase signaling pathways. Mol. Cell Biol. *39*, e00391-18. https://doi.org/10.1128/MCB.00391-18.

Colvin, T.A., Gabai, V.L., Gong, J., Calderwood, S.K., Li, H., Gummuluru, S., Matchuk, O.N., Smirnova, S.G., Orlova, N.V., Zamulaeva, I.A., et al. (2014a). Hsp70-Bag3 interactions regulate cancer-related signaling networks. Cancer Res. *74*, 4731–4740. https://doi.org/10.1158/0008-5472.CAN-14-0747.

Colvin, Teresa A., Gabai, V.L., and Sherman, M.Y. (2014b). Proteotoxicity is not the reason for the dependence of cancer cells on the major chaperone Hsp70. Cell Cycle *13*, 2306–2310. https://doi.org/10.4161/cc.29296.

Coşkun, K.A., Koca, İ., Gümüş, M., and Tutar, Y. (2021). Designing specific HSP70 substrate binding domain inhibitor for perturbing protein folding pathways to inhibit cancer mechanism. Anticancer Agents Med. Chem. *21*, 1472–1480. https://doi.org/10.2174/1871520620666200918103509.

Denoyelle, C., Abou-Rjaily, G., Bezrookove, V., Verhaegen, M., Johnson, T.M., Fullen, D.R., Pointer, J.N., Gruber, S.B., Su, L.D., Nikiforov, M.A., et al. (2006). Anti-oncogenic role of the endoplasmic reticulum differentially activated by mutations in the MAPK pathway. Nat. Cell Biol. *8*, 1053–1063. https://doi.org/10.1038/ncb1471.

Dever, T.E., Feng, L., Wek, R.C., Cigan, A.M., Donahue, T.F., and Hinnebusch, A.G. (1992). Phosphorylation of initiation factor 2 alpha by protein kinase GCN2 mediates gene-specific translational control of GCN4 in yeast. Cell *68*, 585–596. https://doi.org/10.1016/0092-8674(92)90193-g.

Donnelly, N., Gorman, A.M., Gupta, S., and Samali, A. (2013). The eIF2α kinases: their structures and functions. Cell Mol. Life Sci. *70*, 3493–3511. https://doi.org/10.1007/s00018-012-1252-6.

Donnelly, N., and Storchová, Z. (2015). Aneuploidy and proteotoxic stress in cancer. Mol. Cell Oncol. *2*, e976491. https://doi.org/10.4161/23723556.2014.976491.

Doong, H., Price, J., Kim, Y.S., Gasbarre, C., Probst, J., Liotta, L.A., Blanchette, J., Rizzo, K., and Kohn, E. (2000). CAIR-1/BAG-3 forms an EGF-regulated ternary complex with phospholipase C-gamma and Hsp70/Hsc70. Oncogene *19*, 4385–4395. https://doi.org/10.1038/sj.onc.1203797.

Falco, A., Festa, M., Basile, A., Rosati, A., Pascale, M., Florenzano, F., Nori, S.L., Nicolin, V., Di Benedetto, M., Vecchione, M.L., et al. (2012). BAG3 controls angiogenesis through regulation of ERK phosphorylation. Oncogene *31*, 5153–5161. https://doi.org/10.1038/onc.2012.17.

Gabai, V.L., Meng, L., Kim, G., Mills, T.A., Benjamin, I.J., and Sherman, M.Y. (2012). Heat shock transcription factor Hsf1 is involved in tumor progression via regulation of hypoxia-inducible factor 1 and RNA-binding protein HuR. Mol. Cell Biol. *32*, 929–940. https://doi.org/10.1128/MCB.05921-11.

Gabai, V.L., Yaglom, J.A., Waldman, T., and Sherman, M.Y. (2009a). Heat shock protein Hsp72 controls oncogene-induced senescence pathways in cancer cells. Mol. Cell Biol. *29*, 559–569. https://doi.org/10.1128/MCB.01041-08.

Gabai, V.L., Yaglom, J.A., Waldman, T., and Sherman, M.Y. (2009b). Heat shock protein Hsp72 controls oncogene-induced senescence pathways in cancer cells. Mol. Cell Biol. *29*, 559–569. https://doi.org/10.1128/MCB.01041-08.

Gabai, V.L., Yaglom, J.A., Wang, Y., Meng, L., Shao, H., Kim, G., Colvin, T., Gestwicki, J., and Sherman, M.Y. (2016). Anticancer effects of targeting Hsp70 in tumor stromal cells. Cancer Res. *76*, 5926–5932. https://doi.org/10.1158/0008-5472.CAN-16-0800.

Ganassi, M., Mateju, D., Bigi, I., Mediani, L., Poser, I., Lee, H.O., Seguin, S.J., Morelli, F.F., Vinet, J., Leo, G., et al. (2016). A surveillance function of the HSPB8-BAG3-HSP70 chaperone

complex ensures stress granule integrity and dynamism. Mol. Cell *63*, 796–810. https://doi.org/10.1016/j.molcel.2016.07.021.

García, M.A., Gil, J., Ventoso, I., Guerra, S., Domingo, E., Rivas, C., and Esteban, M. (2006). Impact of protein kinase PKR in cell biology: from antiviral to antiproliferative action. Microbiol. Mol. Biol. Rev. *70*, 1032–1060. https://doi.org/10.1128/MMBR.00027-06.

García, M.A., Meurs, E.F., and Esteban, M. (2007). The dsRNA protein kinase PKR: virus and cell control. Biochimie *89*, 799–811. https://doi.org/10.1016/j.biochi.2007.03.001.

Gong, J., Weng, D., Eguchi, T., Murshid, A., Sherman, M.Y., Song, B., and Calderwood, S.K. (2015). Targeting the hsp70 gene delays mammary tumor initiation and inhibits tumor cell metastasis. Oncogene *34*, 5460–5471. https://doi.org/10.1038/onc.2015.1.

Guerriero, L., Palmieri, G., De Marco, M., Cossu, A., Remondelli, P., Capunzo, M., Turco, M.C., and Rosati, A. (2017). The anti-apoptotic BAG3 protein is involved in BRAF inhibitor resistance in melanoma cells. Oncotarget *8*, 80393–80404. https://doi.org/10.18632/oncotarget.18902.

Haeri, M., and Knox, B.E. (2012). Endoplasmic reticulum stress and unfolded protein response pathways: potential for treating age-related retinal degeneration. J. Ophthalmic Vis. Res. *7*, 45–59.

Han, A.-P., Yu, C., Lu, L., Fujiwara, Y., Browne, C., Chin, G., Fleming, M., Leboulch, P., Orkin, S.H., and Chen, J.-J. (2001). Heme-regulated eIF2alpha kinase (HRI) is required for translational regulation and survival of erythroid precursors in iron deficiency. EMBO J. *20*, 6909–6918. https://doi.org/10.1093/emboj/20.23.6909.

Harding, H.P., Zhang, Y., Bertolotti, A., Zeng, H., and Ron, D. (2000). Perk is essential for translational regulation and cell survival during the unfolded protein response. Mol. Cell *5*, 897–904. https://doi.org/10.1016/S1097-2765(00)80330-5.

Harding, H.P., Zhang, Y., and Ron, D. (1999). Protein translation and folding are coupled by an endoplasmic-reticulum-resident kinase. Nature *397*, 271–274. https://doi.org/10.1038/16729.

Harding, H.P., Zhang, Y., Zeng, H., Novoa, I., Lu, P.D., Calfon, M., Sadri, N., Yun, C., Popko, B., Paules, R., et al. (2003). An integrated stress response regulates amino acid metabolism and resistance to oxidative stress. Mol. Cell *11*, 619–633. https://doi.org/10.1016/s1097-2765(03)00105-9.

Hiebel, C., Stürner, E., Hoffmeister, M., Tascher, G., Schwarz, M., Nagel, H., Behrends, C., Münch, C., and Behl, C. (2020). BAG3 proteomic signature under proteostasis stress. Cells *9*, 2416. https://doi.org/10.3390/cells9112416.

Kathage, B., Gehlert, S., Ulbricht, A., Lüdecke, L., Tapia, V.E., Orfanos, Z., Wenzel, D., Bloch, W., Volkmer, R., Fleischmann, B.K., et al. (2017). The cochaperone BAG3 coordinates protein synthesis and autophagy under mechanical strain through spatial regulation of mTORC1. Biochim. Biophys. Acta Mol. Cell Res. *1864*, 62–75. https://doi.org/10.1016/j.bbamcr.2016.10.007.

Kimball, S.R., Clemens, M.J., Tilleray, V.J., Wek, R.C., Horetsky, R.L., and Jefferson, L.S. (2001a). The double-stranded RNA-activated protein kinase PKR is dispensable for regulation of translation initiation in response to either calcium mobilization from the endoplasmic reticulum or essential amino acid starvation. Biochem. Biophys. Res. Commun. *280*, 293–300. https://doi.org/10.1006/bbrc.2000.4103.

Kimball, S.R., Clemens, M.J., Tilleray, V.J., Wek, R.C., Horetsky, R.L., and Jefferson, L.S. (2001b). The double-stranded RNA-activated protein kinase PKR is dispensable for regulation of translation initiation in response to either calcium mobilization from the endoplasmic reticulum or essential amino acid starvation. Biochem. Biophys. Res. Commun. *280*, 293–300. https://doi.org/10.1006/bbrc.2000.4103.

Kögel, D., Linder, B., Brunschweiger, A., Chines, S., and Behl, C. (2020). At the crossroads of apoptosis and autophagy: multiple roles of the co-chaperone BAG3 in stress and therapy resistance of cancer. Cells *9*, 574. https://doi.org/10.3390/cells9030574.

Koren, J., Jinwal, U.K., Jin, Y., O'Leary, J., Jones, J.R., Johnson, A.G., Blair, L.J., Abisambra, J.F., Chang, L., Miyata, Y., et al. (2010). Facilitating Akt clearance via manipulation of Hsp70 activity and levels. J. Biol. Chem. *285*, 2498–2505. https://doi.org/10.1074/jbc.M109.057208.

Kumar, S., Gahramanov, V., Yaglom, J., Patel, S., Kaczmarczyk, L., Alexandrov, I., Gerlitz, G., Salmon-Divon, M., and Sherman, M.Y. (2021). Homologous recombination repair creates mutations in non-coding genome that alter Topoisomerase-1 cleavage sites & orchestrates irinotecan resistance. Preprint at bioRxiv. https://doi.org/10.1101/2021.11.26.470089.

Leu, J.I.-J., Pimkina, J., Frank, A., Murphy, M.E., and George, D.L. (2009). A small molecule inhibitor of inducible heat shock protein 70. Mol. Cell *36*, 15–27. https://doi.org/10.1016/j.molcel.2009.09.023.

Li, X., Colvin, T., Rauch, J.N., Acosta-Alvear, D., Kampmann, M., Dunyak, B., Hann, B., Aftab, B.T., Murnane, M., Cho, M., et al. (2015). Validation of the Hsp70-Bag3 protein-protein interaction as a potential therapeutic target in cancer. Mol. Cancer Ther. *14*, 642–648. https://doi.org/10.1158/1535-7163.MCT-14-0650.

Lu, J., O'Hara, E.B., Trieselmann, B.A., Romano, P.R., and Dever, T.E. (1999). The interferon-induced double-stranded RNA-activated protein kinase PKR will phosphorylate serine, threonine, or tyrosine at residue 51 in eukaryotic initiation factor 2α *. J. Biol. Chem. *274*, 32198–32203. https://doi.org/10.1074/jbc.274.45.32198.

Lu, J., Papp, L.V., Fang, J., Rodriguez-Nieto, S., Zhivotovsky, B., and Holmgren, A. (2006). Inhibition of Mammalian thioredoxin reductase by some flavonoids: implications for myricetin and quercetin anticancer activity. Cancer Res. *66*, 4410–4418. https://doi.org/10.1158/0008-5472.CAN-05-3310.

Massey, A.J., Williamson, D.S., Browne, H., Murray, J.B., Dokurno, P., Shaw, T., Macias, A.T., Daniels, Z., Geoffroy, S., Dopson, M., et al. (2010). A novel, small molecule inhibitor of Hsc70/Hsp70 potentiates Hsp90 inhibitor induced apoptosis in HCT116 colon carcinoma cells. Cancer Chemother. Pharmacol. *66*, 535–545. https://doi.org/10.1007/s00280-009-1194-3.

McCarthy, D.J., Chen, Y., and Smyth, G.K. (2012). Differential expression analysis of multifactor RNA-Seq experiments with respect to biological variation. Nucleic Acids Res. *40*, 4288–4297. https://doi.org/10.1093/nar/gks042.

McEwen, E., Kedersha, N., Song, B., Scheuner, D., Gilks, N., Han, A., Chen, J.-J., Anderson, P., and Kaufman, R.J. (2005). Heme-regulated inhibitor kinase-mediated phosphorylation of eukaryotic translation initiation factor 2 inhibits translation, induces stress granule formation, and mediates survival upon arsenite exposure. J. Biol. Chem. *280*, 16925–16933. https://doi.org/10.1074/jbc.M412882200.

Meng, L., Hunt, C., Yaglom, J.A., Gabai, V.L., and Sherman, M.Y. (2011). Heat shock protein Hsp72 plays an essential role in Her2-induced mammary tumorigenesis. Oncogene *30*, 2836–2845. https://doi.org/10.1038/onc.2011.5.

Meriin, A.B., Narayanan, A., Meng, L., Alexandrov, I., Varelas, X., Cissé, I.I., and Sherman, M.Y. (2018). Hsp70–Bag3 complex is a hub for proteotoxicity-induced signaling that controls protein aggregation. PNAS *115*, E7043–E7052. https://doi.org/10.1073/pnas.1803130115.

Meurs, E., Chong, K., Galabru, J., Thomas, N.B., Kerr, I.M., Williams, B.R., and Hovanessian, A.G. (1990). Molecular cloning and characterization of the human double-stranded RNA-activated protein kinase induced by interferon. Cell *62*, 379–390. https://doi.org/10.1016/0092-8674(90)90374-n.

Moradi-Marjaneh, R., Paseban, M., and Moradi Marjaneh, M. (2019). Hsp70 inhibitors: implications for the treatment of colorectal cancer. IUBMB Life *71*, 1834–1845. https://doi.org/10.1002/iub.2157.

Mosser, D.D., and Morimoto, R.I. (2004). Molecular chaperones and the stress of oncogenesis. Oncogene *23*, 2907–2918. https://doi.org/10.1038/sj.onc.1207529.

Mukherjee, T., Ramaglia, V., Abdel-Nour, M., Bianchi, A.A., Tsalikis, J., Chau, H.N., Kalia, S.K., Kalia, L.V., Chen, J.-J., Arnoult, D., et al. (2021). The eIF2α kinase HRI triggers the autophagic clearance of cytosolic protein aggregates. J. Biol. Chem. *296*, 100050. https://doi.org/10.1074/jbc.RA120.014415.

Pakos-Zebrucka, K., Koryga, I., Mnich, K., Ljujic, M., Samali, A., and Gorman, A.M. (2016). The integrated stress response. EMBO Rep. *17*, 1374–1395. https://doi.org/10.15252/embr.201642195.

Phillips, P.A., Sangwan, V., Borja-Cacho, D., Dudeja, V., Vickers, S.M., and Saluja, A.K. (2011). Myricetin induces pancreatic cancer cell death via the induction of apoptosis and inhibition of the phosphatidylinositol 3-kinase (PI3K) signaling pathway. Cancer Lett. *308*, 181–188. https://doi.org/10.1016/j.canlet.2011.05.002.

Pirali, M., Taheri, M., Zarei, S., Majidi, M., and Ghafouri, H. (2020). Artesunate, as a HSP70 ATPase activity inhibitor, induces apoptosis in breast cancer cells. Int. J. Biol. Macromol. *164*, 3369–3375. https://doi.org/10.1016/j.ijbiomac.2020.08.198.

Rérole, A.-L., Gobbo, J., De Thonel, A., Schmitt, E., Pais de Barros, J.P., Hammann, A., Lanneau, D., Fourmaux, E., Deminov, O., Micheau, O., et al. (2011). Peptides and aptamers targeting HSP70: a novel approach for anticancer chemotherapy. Cancer Res. *71*, 484–495. https://doi.org/10.1158/0008-5472.CAN-10-1443.

Ritchie, M.E., Phipson, B., Wu, D., Hu, Y., Law, C.W., Shi, W., and Smyth, G.K. (2015). Limma powers differential expression analyses for RNA-sequencing and microarray studies. Nucleic Acids Res. *43*, e47. https://doi.org/10.1093/nar/gkv007.

Robinson, M.D., McCarthy, D.J., and Smyth, G.K. (2010). edgeR: a Bioconductor package for differential expression analysis of digital gene expression data. Bioinformatics *26*, 139–140. https://doi.org/10.1093/bioinformatics/btp616.

Ron, D. (2002). Proteotoxicity in the endoplasmic reticulum: lessons from the Akita diabetic mouse. J. Clin. Invest. *109*, 443–445. https://doi.org/10.1172/JCI15020.

Rosati, A., Basile, A., Falco, A., d'Avenia, M., Festa, M., Graziano, V., De Laurenzi, V., Arra, C., Pascale, M., and Turco, M.C. (2012). Role of BAG3 protein in leukemia cell survival and response to therapy. Biochim. Biophys. Acta *1826*, 365–369. https://doi.org/10.1016/j.bbcan.2012.06.001.

Shao, H., Li, X., Moses, M.A., Gilbert, L.A., Kalyanaraman, C., Young, Z.T., Chernova, M., Journey, S.N., Weissman, J.S., Hann, B., et al. (2018). Exploration of benzothiazole-rhodacyanines as allosteric inhibitors of protein-protein interactions with heat shock protein 70 (Hsp70). J. Med. Chem. *61*, 6163–6177. https://doi.org/10.1021/acs.jmedchem.8b00583.

Sherman, M.Y., and Gabai, V.L. (2015). Hsp70 in cancer: back to the future. Oncogene *34*, 4153–4161. https://doi.org/10.1038/onc.2014.349.

Solimini, N.L., Luo, J., and Elledge, S.J. (2007). Non-oncogene addiction and the stress phenotype of cancer cells. Cell *130*, 986–988. https://doi.org/10.1016/j.cell.2007.09.007.

Tabas, I., and Ron, D. (2011). Integrating the mechanisms of apoptosis induced by endoplasmic reticulum stress. Nat. Cell Biol. *13*, 184–190. https://doi.org/10.1038/ncb0311-184.

Tao, Y., Messer, J.S., Goss, K.H., Hart, J., Bissonnette, M., and Chang, E.B. (2016). Hsp70 exerts oncogenic activity in the Apc mutant Min mouse model. Carcinogenesis *37*, 731–739. https://doi.org/10.1093/carcin/bgw056.

Thulasiraman, V., Xu, Z., Uma, S., Gu, Y., Chen, J.J., and Matts, R.L. (1998). Evidence that Hsc70 negatively modulates the activation of the heme-regulated eIF-2alpha kinase in rabbit reticulocyte lysate. Eur. J. Biochem. *255*, 552–562. https://doi.org/10.1046/j.1432-1327.1998.2550552.x.

Thulasiraman, V., Yun, B.-G., Uma, S., Gu, Y., Scroggins, B.T., and Matts, R.L. (2002). Differential inhibition of Hsc70 activities by two Hsc70-binding peptides. Biochemistry *41*, 3742–3753. https://doi.org/10.1021/bi012137n.

Ulbricht, A., Eppler, F.J., Tapia, V.E., van der Ven, P.F.M., Hampe, N., Hersch, N., Vakeel, P., Stadel, D., Haas, A., Saftig, P., et al. (2013). Cellular mechanotransduction relies on tension-induced and chaperone-assisted autophagy. Curr. Biol. *23*, 430–435. https://doi.org/10.1016/j.cub.2013.01.064.

Walter, P., and Ron, D. (2011). The unfolded protein response: from stress pathway to homeostatic regulation. Science *334*, 1081–1086. https://doi.org/10.1126/science.1209038.

Wang, Z., Song, T., Guo, Z., Uwituze, L.B., Guo, Y., Zhang, H., Wang, H., Zhang, X., Pan, H., Ji, T., et al. (2021). A novel Hsp70 inhibitor specifically targeting the cancer-related Hsp70-Bim protein-protein interaction. Eur. J. Med. Chem. *220*, 113452. https://doi.org/10.1016/j.ejmech.2021.113452.

Wek, R.C. (2018). Role of eIF2α kinases in translational control and adaptation to cellular stress. Cold Spring Harb. Perspect. Biol. *10*, a032870. https://doi.org/10.1101/cshperspect.a032870.

Yaglom, J.A., Gabai, V.L., and Sherman, M.Y. (2007). High levels of heat shock protein Hsp72 in cancer cells suppress default senescence pathways. Cancer Res. *67*, 2373–2381. https://doi.org/10.1158/0008-5472.CAN-06-3796.

Yaglom, J.A., McFarland, C., Mirny, L., and Sherman, M.Y. (2014). Oncogene-triggered suppression of DNA repair leads to DNA instability in cancer. Oncotarget *5*, 8367–8378. https://doi.org/10.18632/oncotarget.2259.

Yaglom, J.A., Wang, Y., Li, A., Li, Z., Monti, S., Alexandrov, I., Lu, X., and Sherman, M.Y. (2018). Cancer cell responses to Hsp70 inhibitor JG-98: comparison with Hsp90 inhibitors and finding synergistic drug combinations. Sci. Rep. *8*, 3010. https://doi.org/10.1038/s41598-017-14900-0.

Yerlikaya, A., Kimball, S.R., and Stanley, B.A. (2008). Phosphorylation of eIF2α in response to 26S proteasome inhibition is mediated by the haem-regulated inhibitor (HRI) kinase. Biochem. J. *412*, 579–588. https://doi.org/10.1042/BJ20080324.

STAR★METHODS

KEY RESOURCES TABLE

REAGENT or RESOURCE	SOURCE	IDENTIFIER
Antibodies		
Phospho-eIF2a_Ser51	Cell Signaling Technology	Cat# 3597; RRID:AB_390740
EIF2AK1/HRI	Proteintech	Cat# 20499-1-AP; RRID:AB_10697665
EIF2AK1/HRI	Abcam	Cat# ab28530; RRID:AB_869595
Anti-Bag3	Proteintech	Cat# 10599-1-AP; RRID:AB_2062602
β-actin	Novus	Cat# NB600-501; RRID:AB_10077656
a-K48 Ubiquitin linkage antibody	BostonBiochem	Cat#A101-050; RRID:AB_2894847
Chemicals, peptides, and recombinant proteins		
JG98	AdooQ BIOSCIENCE	Catalog No.: A18734
MG132	Biomol	LKT-M2400.5
DAPI (4′,6-Diamidine-2′-phenylindole dihydrochloride)	Sigma	Cat# 10236276001
Formaldehyde	Sigma	Cat#FX0415
Blasticidin S HCl	Thermo Fisher	Cat# A1113903
Recombinant Human His6-Ubiquilin-1 Tandem UBA	BostonBiochem	UBE110
Qiagen RNeasy Plus Mini kit	Qiagen;GmbH	Cat. #74134
qScript cDNA Synthesis Kit	Quanta Bio	Cat. #95047-100
PerfeCTa SYBR Green FastMix ROX	Quanta Bio	Cat. #95073-012
DMEM/F-12 1:1	BI-Biologicals	Cat# 01-170-1A
horse serum	BI-Biologicals	Cat. #04-0041A
epidermal growth factor	Peprotech	Cat. #AF-100-15
Hydrocortisone	Sigma	Cat. #H-0888
human insulin	Sigma	Cat. #I9278
cholera toxin	Sigma	Cat. #C-8052
Fetal Bovine Serum	BI-Biologicals	Cat. #04-007-1A
L-glutamine	BI-Biologicals	Cat. #03-020-1B
L-alanyl-L-glutamine	BI-Biologicals	Cat. #03-022-1B
Penstrep	BI-Biologicals	Cat. #03-031-1B
HisPur Ni-NTA Resin	ThermoFisher Scientific	Cat. #88221
RNeasy Mini kit	Qiagen	Cat. #74104
Deposited data		
Transcriptome analysis	GEO	GSE171440
Experimental models: cell lines		
MCF10A (human breast epithelial)	ATCC	Cat# CRL-10317; RRID:CVCL_0598
HEK293T	ATCC	Cat# CRL-3216, RRID:CVCL_0063
Oligonucleotides		
Supplement table	See Tables S3 and S4	N/A
Software and algorithms		
Hermes Wiscon Imaging System with Athena Winsoft software package (V1.0.10)	IDEA Bio-Medical Ltd	RRID:SCR_021786
Fiji-ImageJ	ImageJ	RRID:SCR_002285
limma package	R-package	LIMMA, RRID:SCR_010943

(Continued on next page)

Continued

REAGENT or RESOURCE	SOURCE	IDENTIFIER
Gene Set Enrichment Analysis	Broad Institute	RRID:SCR_003199
GraphPad Prism_v9	GraphPad Software Inc	GraphPad Prism, RRID:SCR_002798
trim_galore_v0.5.0	Babraham Bioinformatics	Trim Galore, RRID:SCR_011847
FastQC_v0.11.7	Babraham Bioinformatics	FastQC, RRID:SCR_014583
Hisat2_v2.1.0	daehwankimlab	HISAT2, RRID:SCR_015530
GRch38.97	UCSC	NA
samtools_v1.9	N/A	SAMTOOLS, RRID:SCR_002105
featureCounts_v1.6.3	N/A	featureCounts, RRID:SCR_012919
Bioconductor packages	Bioconductor	RRID:SCR_006442

RESOURCE AVAILABILITY

Lead contact

Further information and requests for resources should be directed to and will be fulfilled by the lead contact, Shivani Patel (shivanip@ariel.ac.il, patel.shiva2593@gmail.com).

Materials availability

This study did not generate new unique reagents.

Data and code availability

All data supporting the findings of this publication can be found within the supporting information and the primary publication except those noted here. The transcriptome analysis related raw FASTQ files, count file and differentially expressed gene list can be accessed via accession number GSE171440 at GEO database (Gene Expression Omnibus (GEO), RRID:SCR_005012). Codes for analysis of transcriptome analysis was used as indicated (Kumar et al., 2021).

Image illustrations: Created with BioRender.com (Academic license and permissions attached).

EXPERIMENTAL MODEL AND SUBJECT DETAILS

Cell culture

MCF10A (human breast epithelial, ATCC Cat# CRL-10317, RRID:CVCL_0598) cells were grown in DMEM/F-12 1:1 (Cat# 01-170-1A, Biological Industries) medium supplemented with 5% horse serum (Cat. #04-0041A, BI-Biologicals), 20 ng/mL epidermal growth factor (Cat. #AF-100-15,Peprotech, 1 mg), 0.5 μg/mL hydrocortisone(Cat. #H-0888, Sigma), 10 μg/mL human insulin (Cat. #I9278, Sigma), and 100 ng/mL cholera toxin (Cat. #C-8052, Sigma). HEK293 T (ATCC Cat# CRL-3216, RRID:CVCL_0063) cells were grown in DMEM high glucose with 10% Fetal Bovine Serum (FBS, Cat. #04-007-1A, BI-Biologicals). All cultures were supplemented with L-glutamine (Cat. #03-020-1B, BI-Biologicals), L-alanyl-L-glutamine (Cat. #03-022-1B, BI-Biologicals), penstrep (Cat. #03-031-1B, BI-Biologicals), and were grown in a humidified incubator at 37°C and 5% CO2 (Meriin et al., 2018). Cell cultures were checked for mycoplasma contamination routinely at six-week intervals.

METHOD DETAILS

Reagents and antibodies

JG98 was purchased from AdooQ BIOSCIENCE (Catalog No.: A18734), MG132 from Biomol (LKT-M2400.5), 6% formaldehyde (Cat#FX0415) and DAPI (4′,6-Diamidine-2′-phenylindole dihydrochloride, Cat# 10236276001) from Sigma, Blasticidin S HCl (Cat# A1113903) from Thermo Fisher Scientific. Antibodies against, Phospho-eIF2α_Ser51 (Cell Signaling Technology Cat# 3597, RRID:AB_390740); EIF2AK1/HRI- (Proteintech Cat# 20499-1-AP, RRID:AB_10697665) or EIF2AK1/HRI- (Abcam Cat# ab28530, RRID:AB_869595), anti-Bag3 (Proteintech Cat# 10599-1-AP, RRID:AB_2062602) and β-actin (Novus Cat# NB600-501, RRID:AB_10077656), α-K48 Ubiquitin linkage antibody (RRID:AB_2894847, Cat#A101-050), Recombinant Human His6-Ubiquilin-1 Tandem UBA (UBE110) were from Boston Biochem.

Constructs and oligonucleotides

The retroviral expression vector pCXbsr containing Her2/NeuT was described previously (Yaglom et al., 2014). For pull-down experiments we used pcDNA3.1-based plasmids used for overexpression of N-terminally His-tagged Bag3 Full length described previously (T.A. Colvin et al., 2014a; Meriin et al., 2018).

We used the following siGENOME siRNAs purchased from Dharmacon (Supplement table): nontargeting siRNA no. 5, BAG3 (D-011957-01), GCN2 (D-016634-02), DDIT3 (M-017609-01), HRI (M-006968-00) , siPERK (sc-36213) and siPKR (sc-36263) from Santa Cruz, see also Table S3.

Real time PCR analysis

Total RNA was isolated from cells using Qiagen RNeasy Plus Mini kit (Cat. #74134; GmbH). The qScript cDNA Synthesis Kit (Quanta Bio, Cat. #95047-100) was used to convert 1ug mRNA into cDNA. qRT–PCR was performed using the PerfeCTa SYBR Green FastMix ROX (Quanta Bio, Cat. #95073-012) according to the manufacture's protocols; expression levels of β-Actin were used as an internal control. Real-time analysis was performed with a AriaMx Real-Time PCR System (Agilent AriaMx Real-time PCR System, RRID:SCR_019469) instrument using the primers (Supplement table) from Integrated DNA technologies (IDT), Belgium. For primer details see also Table S4.

Virus preparation and infection

Retroviral expression vector pCXbsr expressing HER2/Neu gene under Blasticidin S HCl (Cat# A1113903) from Thermo Fisher Scientific was used. Only pCXbsr without any insert was used as an 'empty or E' vector control. Retroviruses were produced as reported before (Gabai et al., 2009b; Yaglom et al., 2014). Briefly, HEK293 T cells were co-transfected with plasmids expressing retroviral proteins Gag-Pol, Vesicular somatitis virus G glycoprotein and our gene of interest or enhanced green fluorescent protein (Gabai et al., 2009b) using Lipofectamine 3000 (Cat. #L3000015,Invitrogen, Boston, USA). After 48 hours of transfection, supernatants containing the retroviral particles were collected, aliquoted, and frozen at −80°C until use. Cells were infected with diluted supernatant in the presence of 8 μg/mL Polybrene overnight, and were selected with blasticidin (10 μg/mL) 48 h after infection. Retroviral vectors expressing enhanced green fluorescent protein was used as infection efficiency indicator: virus dilution was used to achieve approximately 90% of infected cells being GFP positive 2 days after infection. Transformation of Neu/Her2 was also quantified through qPCR represented by Cq(ΔR) values (See also Figure S1).

Immunofluorescence

Cells were fixed at room temperature (RT) using 4% paraformaldehyde for 5 min and permeabilized at RT in 0.2% Triton X-100 in PBS for 10 min. Cells were washed two times with PBST (1xPBS,0.05%Tween) and incubated with DAPI (1:10000) for 5 min at RT, followed by three additional washes with PBST. Imaging was performed at 20x, blue channel (Ex. 390/22, Em. 440/40) using Hermes Wiscon Imaging System (IDEA Bio-Medical Ltd., WiScan Hermes High Content Imaging System, RRID:SCR_021786) that captured numerous images per well listed in respective figure legends. Image analysis was performed using inbuilt software package system (Athena Wisoft, Ver: V1.0.10).

Immunoprecipitation and immunoblotting

Cells were lysed with lysis buffer (50 mM Tris-HCl (pH 7.4), 150 mM NaCl, 1% Triton X-100, 5 mM EDTA, 1 mM Na3VO4, 50 mM β-glycerophosphate, 50 mM NaF) supplemented with Protease Inhibitor Cocktail (Cat. #P8340, Sigma) and Phenylmethylsulfonyl fluoride (PMSF). Samples were adjusted to have equal concentration of total protein and subjected to PAGE electrophoresis followed by immunoblotting with respective antibodies (Meriin et al., 2018).

Raw images of immunoprecipitation and immunoblotting

Please refer Data S1 for raw data images. All the images presented in current manuscript has been availed as separate supplement file.

Pull-down experiments

For pull-down analysis of Bag3 and associated proteins, HEk293 T cells were transfected in 10 cm dishes with full length Bag3 construct, treated with different conditions. The cells were washed with DPBS, fixed with 1.2% formaldehyde for 10 minutes at room temperature, then Tris-HCl (pH 7.4) was added to 50 mM

final concentration which was followed by a wash with 50 mM Tris-HCl (pH 7.4) in DPBS at 4°C. The cells were lysed in: DPBS (BI Biologicals) supplemented with 30 mM NaCl, 10 mM Hepes (pH 7.4), 1.5 mM MgCl2 , 0.5% Triton X-100, 5% glycerol, 10 mM imidazole, 1 mM PMSF and Protease Inhibitor Cocktails (Sigma: P8849). All steps were carried out at 4°C. The lysates were passed 3 times through a syringe (21G needle), clarified by centrifugation for 7 minutes at 16,000x g. The supernatants were adjusted to have equal concentration of total protein and loaded on 15 μl of HisPur Ni-NTA Resin (Cat. #88221,ThermoFisher Scientific). After incubation for 40 minutes, the flow through was allowed to pass through the beads twice more, and the beads were washed five times with DPBS supplemented with 146 mM NaCl, 20 mM Tris-HCl (pH 8.0), 0.5% Triton X-100, 5% glycerol, 15 mM imidazole. The His-tagged Bag3 along with associated proteins was eluted with 300 mM imidazole in 50 mM Na(PO4) (pH 6.8), 300 mM NaCl. The eluted samples were immunoblotted with respective antibodies (Meriin et al., 2018).

For pull-down analysis of ubiquitinated polypeptides, MCF10A (Untransformed) cells plated on 10 cm dish and treated with JG-98 for 12 hours or left untreated. After that cell were washed with DPBS and fixed with 1.2% formaldehyde followed by a wash with 50 mM Tris-HCl (pH 7.4) in DPBS at 4°C. The cells were lysed in: DPBS (BI Biologicals) supplemented with 30 mM NaCl, 10 mM Hepes (pH 7.4), 1.5 mM $MgCl_2$, 0.5% Triton X-100, 5% glycerol, 10 mM imidazole, 1 mM PMSF and Protease and Phosphatase Inhibitor Cocktails (Sigma: P8340). All steps were performed at 4°C and clarified by centrifugation for 7 minutes at 16,000x g. The supernatants were adjusted to have equal concentration of total protein and then supplemented with 10 μg of His6-Ubiquilin-1 Tandem UBA (BostonBiochem: UBE-110). After incubation for 60 minutes, 15 μl of HisPur Cobalt Resin (Pierce, ThermoFisher Scientific) were added, and all the following steps described for the His-tagged Bag3 pull-down were performed (Meriin et al., 2018).

Data analysis

Hermes Wiscon Imaging System with Athena Winsoft software package (V1.0.10) was used for immunofluorescence experiments. Fiji-ImageJ (Fiji, RRID:SCR_002285) was used for all quantification of immunoblotting. Transcriptome analysis was done using pipeline developed inhouse, differentially expressed genes were computed through limma package (LIMMA, RRID: SCR_010943), (McCarthy et al., 2012; Ritchie et al., 2015; Robinson et al., 2010). Further gene enrichment was computed using the Broad Institute software package for gene set enrichment analysis (Gene Set Enrichment Analysis, RRID:SCR_003199), Also, R studio packages and GraphPad Prism_v9 (GraphPad Prism, RRID:SCR_002798) was used to compute statistical parameters and plotting. Statistical analysis was performed by Student's t test, one-way analysis of variance (ANOVA), or two-way ANOVA as appropriate. Data were expressed as means ± SEM.

RNAseq processing

RNA was extracted from cells using the RNeasy Mini kit (Cat. #74104, Qiagen). Library preparation strategy (BGISEQ-500) was adopted and performed by BGI, China.

Data processing

We developed our own pipeline to analyze the data where reads were first trimmed and clipped for quality control in trim_galore_v0.5.0 (Trim Galore, RRID:SCR_011847) and checked for each sample using FastQC_v0.11.7 (FastQC, RRID:SCR_014583). Data was aligned by Hisat2_v2.1.0 (HISAT2, RRID: SCR_015530) using hg38, GRch38.97. High-quality reads were then imported into samtools_v1.9 using htslib 1.9 (SAMTOOLS, RRID:SCR_002105) conversion to BAM file. Gene-count summaries were generated with featureCounts_v1.6.3 (featureCounts, RRID:SCR_012919): A numeric matrix of raw read counts was generated, with genes in rows and samples in columns, and used for differential gene expression analysis with the Bioconductor packages (Bioconductor, RRID:SCR_006442), (McCarthy et al., 2012; Ritchie et al., 2015; Robinson et al., 2010).